



Matrix diffusion rates in fractured volcanic rocks at the Nevada Test Site: Evidence for a dominant influence of effective fracture apertures

Paul W. Reimus¹ and Timothy J. Callahan²

Received 16 November 2006; revised 16 November 2006; accepted 27 March 2007; published 13 July 2007.

[1] Solute matrix diffusion in saturated, fractured volcanic rock at the Nevada Test Site was evaluated from field tracer tests conducted at two different locations and from laboratory-scale transport experiments using core samples from the two locations. The laboratory tests included 15 separate tracer transport experiments conducted in 8 fractured cores (4 from each location) and 17 diffusion cell experiments conducted in matrix material adjacent to the fractures. All of the experiments featured two nonsorbing tracers with free diffusion coefficients differing by a factor of approximately 3 to allow the effects of diffusion to be distinguished from the effects of advection, dispersion, and source-term tailing in the experiments. When considering all the laboratory and field transport experiments collectively, the lumped mass transfer parameter that characterizes matrix diffusion rates, $\frac{\phi_m}{b} \sqrt{D_m}$ ($\text{sec}^{-1/2}$) (where ϕ_m is the matrix porosity, b is the effective fracture half-aperture, and D_m is the matrix diffusion coefficient), appears to decrease as time and length scales of observation increase. However, these decreasing trends largely disappear when the laboratory and field data are considered separately, and there is little difference in D_m values measured at different timescales in laboratory experiments using the same rocks. Also, the overall variability in ϕ_m and D_m in the laboratory experiments is not large enough to account for the order-of-magnitude smaller field-scale values of $\frac{\phi_m}{b} \sqrt{D_m}$ compared to lab-scale values. We conclude that experimentally observed trends of $\frac{\phi_m}{b} \sqrt{D_m}$ versus time or distance scale in saturated fractured rocks at the Nevada Test Site are dominated by differences in effective fracture apertures in the various experiments, with a tendency toward larger apertures in the field experiments. These results underscore the importance of acquiring a better understanding of the factors that control effective fracture apertures as a function of distance scale in fractured media if values of $\frac{\phi_m}{b} \sqrt{D_m}$ from laboratory and field tracer experiments are to be reliably extrapolated to time and distance scales in risk assessment models.

Citation: Reimus, P. W., and T. J. Callahan (2007), Matrix diffusion rates in fractured volcanic rocks at the Nevada Test Site: Evidence for a dominant influence of effective fracture apertures, *Water Resour. Res.*, 43, W07421, doi:10.1029/2006WR005746.

1. Introduction

[2] In fractured rock groundwater systems, it is well known that the diffusive mass transfer of solutes between flowing water in fractures and relatively stagnant water in the surrounding rock matrix (matrix diffusion) can significantly retard the movement of solutes through the flow system [Neretnieks, 1980; Grisak and Pickens, 1980; Tang et al., 1981; Maloszewski and Zuber, 1984; Moreno and Neretnieks, 1993; Robinson, 1994]. Therefore accounting for matrix diffusion is critical in assessing contaminant migration in fractured rock groundwater systems. The objective of this

paper is to examine the experimental and observational evidence for scaling behavior of matrix diffusion in saturated fractured media at the Nevada Test Site (NTS) and to explore explanations for apparent scaling trends.

[3] We make a distinction between parameters that affect “rates” of matrix diffusion (matrix diffusion coefficients, matrix porosity, effective fracture apertures) and geometric parameters that affect diffusion “length scales” (matrix block sizes and shapes, flowing fracture spacing). Although both types of parameters are critical for properly modeling matrix diffusion at risk assessment scales, we address only the parameters that affect rates in this paper because diffusion length scales could not be estimated in any of the field experiments discussed herein because of practical time constraints. Even for relatively large solute matrix diffusion coefficients of $\sim 5 \times 10^{-6} \text{ cm}^2/\text{s}$, the approximate matrix penetration distance ($\sqrt{2D_m t}$) for a diffusing solute in a tracer experiment with a mean tracer residence time of 1 year is only about 18 cm, which is still quite small relative

¹Earth and Environmental Sciences Division, Los Alamos National Laboratory, Los Alamos, New Mexico, USA.

²Department of Geology and Environmental Geosciences, College of Charleston, Charleston, South Carolina, USA.

to flowing fracture spacings and matrix block sizes in fractured rock aquifers at the NTS [Bechtel-SAIC Corporation, 2004b]. Thus, unless extremely long experiments/observations or highly detailed hydrogeologic characterizations are performed, matrix diffusion length scales in fractured rock aquifers are probably best addressed in risk assessment models through sensitivity analyses using alternative conceptual model geometries.

[4] The conceptual model most often used to describe solute transport through fractured geologic media is the “dual-porosity” or “dual-region” model in which the flow domain is divided into two regions that have a large contrast in permeability such that flow is negligible in one of the regions [Tsang, 1995; Lichtner, 2000]. There are two main variants of dual-porosity models, those in which diffusive mass transfer of solutes between flowing and nonflowing regions is described explicitly using diffusion equations within the nonflowing porosity [e.g., Neretnieks, 1980; Grisak and Pickens, 1980; Tang et al., 1981; Maloszewski and Zuber, 1984; Callahan et al., 2000; Becker and Shapiro, 2000; Reimus et al., 2003a, 2003b], and those in which the diffusive mass transfer is approximated using reversible first-order rate expressions to account for mass transfer between the flowing and nonflowing regions [Toride et al., 1995; Bajracharya and Barry, 1997; Maraga et al., 1999; and references therein].

[5] In the former approach, the mass transport equations for a nonreacting solute (assuming a parallel-plate fracture system with one-dimensional flow coupled with diffusion into matrix blocks perpendicular to the flow direction) are:

$$\text{Flowing Region : } \frac{\partial C}{\partial t} + V \frac{\partial C}{\partial x} - D \frac{\partial^2 C}{\partial x^2} - \frac{\phi_m}{b} D_m \frac{\partial C_m}{\partial y} \Big|_{y=b} = 0 \quad (1)$$

$$\text{Nonflowing Region : } \frac{\partial C_m}{\partial t} - D_m \frac{\partial^2 C_m}{\partial y^2} = 0 \quad (2)$$

where

C = solute concentration in fractures or flowing porosity, grams per cubic centimeter

C_m = solute concentration in matrix or nonflowing porosity, grams per cubic centimeter

V = mean water velocity in fractures, centimeters per second

D = solute dispersion coefficient in fractures, square centimeters per second

ϕ_m = matrix porosity

b = fracture half aperture, centimeters (fractures assumed to have an internal porosity of 1.0)

D_m = solute diffusion coefficient in matrix, square centimeters per second
 x = coordinate in flow direction,
 y = coordinate in diffusion direction, and

t = time, seconds.

We note here that the fracture half aperture b is equivalent to the volume to surface area ratio that tracers or contaminants experience in a fracture, which effectively generalizes equations (1) and (2) to apply to rough-walled fractures as well as parallel-plate fractures. The inverse of b is

sometimes referred to as the “flow-wetted surface area per unit volume” [Moreno and Neretnieks, 1993].

[6] In the latter approach, the equations are:

Flowing Region : Flowing Region :

$$\frac{\partial C}{\partial t} + V \frac{\partial C}{\partial x} - D \frac{\partial^2 C}{\partial x^2} - \beta(C - C_m) = 0 \quad (3)$$

$$\text{Nonflowing Region : } \frac{\partial C_m}{\partial t} + \frac{\phi_m}{\phi_f} \beta(C_m - C) = 0 \quad (4)$$

where,

β = first-order mass transfer coefficient between flowing and nonflowing regions, per second,

ϕ_m = “overall” matrix (nonflowing) porosity, and

ϕ_f = overall flowing porosity.

Equations (1)–(4) can take on slightly different forms depending on the flow geometry (for example, linear versus radial flow) and the assumed geometry of the matrix blocks (for example, rectangular, cylindrical, spherical, or other-shaped blocks), but the basic concepts remain the same. We use a linear flow model with rectangular blocks for discussion and analysis purposes, as these assumptions provide the simplest equations. Equations (3) and (4) contain an explicit mass transfer coefficient, and it can be shown [Reimus et al., 2003b] that a similar mass transfer coefficient for equations (1) and (2) is given by $\frac{\phi_m}{b} \sqrt{D_m}$ ($\text{sec}^{-1/2}$). The square of this lumped parameter has the same units as β in equations (3) and (4).

[7] It can be shown [Rao et al., 1980] that because equations (3) and (4) do not explicitly account for diffusion length scales or concentration profiles that develop and change over time in the nonflowing porosity, β must decrease approximately linearly with increasing timescale to accurately model matrix diffusion. We wish to avoid any apparent scale dependence of matrix diffusion mass transfer rates that result from mathematical approximations, so we will use equations (1) and (2) and the mass transfer parameter $\frac{\phi_m}{b} \sqrt{D_m}$ to represent matrix diffusion rates in fractured rock.

[8] It should be pointed out that Haggerty and Gorelick [1995] showed that “multiple” first-order mass transfer expressions similar to the one in equations (3) and (4) with appropriately selected rate constants can yield the same results as the explicit diffusion equations in a variety of matrix configurations and can also approximate diffusion behavior governed by a “distribution” of matrix diffusion rates. However, the data sets discussed in this paper were all fitted well assuming a single matrix diffusion rate, and given our objectives of comparing diffusion rates at different scales, we felt justified in avoiding the additional complexity associated with multirate diffusion.

[9] In this paper, we use data obtained from field and laboratory studies conducted over the past 10 years at the NTS to characterize solute transport processes in saturated, fractured volcanic rock. The studies collectively provide a data set obtained over a wide range of time and length scales in rocks of similar characteristics, which avoids the complications that arise when considering data from significantly different geologic settings. Two locations were studied in detail, the UE-25 C wells complex, completed in layered ash flow tuffs just southeast of the proposed high-

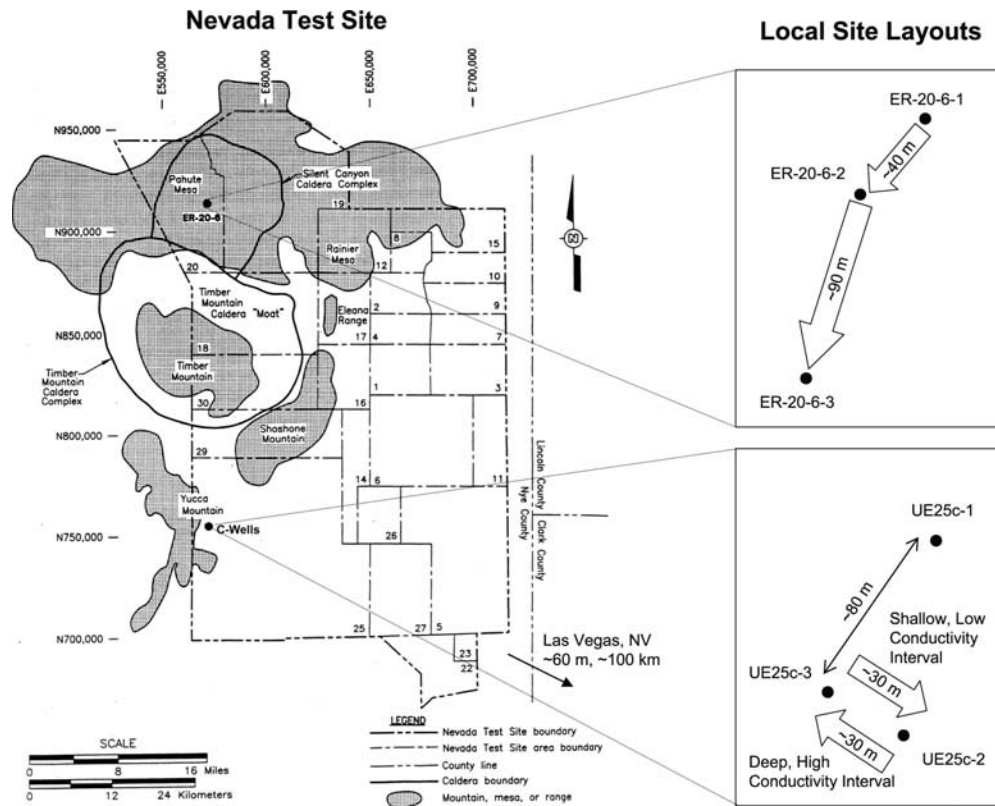


Figure 1. Location and layout of the two field test sites at which paired tracer tests were conducted (solid gray corresponds to mountain ranges or mesas, textured gray corresponds to major basins). The large arrows indicate the tracer transport directions and distances. It is ~60 miles (~100 km) from the southeast corner of the Test Site to downtown Las Vegas.

level nuclear waste repository at Yucca Mountain, and the ER-20-6 complex, completed in volcanic tuffs and lavas on Pahute Mesa, where underground nuclear tests were conducted for many years. The C wells were constructed for investigating solute transport processes to support predictive modeling of radionuclide transport from the proposed Yucca Mountain nuclear waste repository, and the ER-20-6 complex was completed for investigations to support predictive modeling of radionuclide transport from underground nuclear test cavities on Pahute Mesa. The hydrogeology at both locations is dominated by fracture flow within a rock matrix that ranges in total porosity from about 0.10 to 0.35. Figure 1 shows the locations and layouts of the two well complexes, as well as the interwell transport directions and distances in the field tests.

[10] Two separate multiple-tracer tests were conducted at two different depth intervals at the C wells, and a single test involving tracer injections into two different wells was conducted at the ER-20-6 complex. For details of the C-wells field tracer tests and their interpretations, the reader is referred to the works of *Reimus et al.* [2003a] and *Bechtel-SAIC Corporation* [2004a], and for details of the ER-20-6 field tracer tests, the reader is referred to the works of *Reimus and Haga* [1999] and *International Technology (IT) Corporation* [1998].

[11] To help constrain interpretations of the field tracer tests, laboratory experiments were conducted in cores obtained from the field test intervals in both the C wells and ER-20-6-1. These cores were selected to represent

different lithologies (ranging from welded devitrified tuffs or lava flows of low matrix porosity to nonwelded or partially welded devitrified tuffs or lava flows of high matrix porosity) present in the relatively long field test intervals (80 m or more in each test). The laboratory experiments included tracer tests conducted in both induced fractures (C wells) and naturally fractured cores (ER-20-6-1), with fractures running axially down the length of the cores, as well as diffusion cell experiments conducted using intact matrix samples of known thickness and cross-sectional area that were taken from the same cores as the fractures. The experimental methods and results are described in detail by *Callahan et al.* [2000], *Callahan* [2001], and *Bechtel-SAIC Corporation* [2004a] for the C wells site and by *Reimus et al.* [2002a] for the ER-20-6 site. However, these experimental results were reinterpreted for this paper to improve the consistency in the methods of estimating $\frac{\phi_m}{b} \sqrt{D_m}$ from the lab and field data and from the data from the different sites (the data themselves remained the same). Previously, there were differences in the fitting constraints and objective functions that resulted in subtle biases in the parameter estimates, which cast doubts on comparisons of the parameters obtained from the different data sets.

2. Methods

[12] While the experimental and interpretive methods are described in detail in the references cited in the two preceding paragraphs, we emphasize the following points

Table 1. Properties and Dimensions of Fractured Cores and Flow Rates Used in Fracture Transport Experiments

Fractured Core Well, Depth, m bgs	Designator in Figures 2–5	Matrix Porosity	Fracture Length, cm	Core Diameter, cm	Fast Flow Rate, mL/h	Slow Flow Rate, mL/h
UE-25C-2, 533	A	0.272	16.1	9.5	3.8	0.51
UE-25C-2, 553	B	0.138	17.3	9.5	5.9	0.44
UE-25C-1, 573	C	0.288	11.6	9.5	11.4	0.46
UE-25C-1, 795	D	0.298	21.7	9.5	5.0	0.47
ER-20-6-1, 682	E	0.297	25.4	12.7	9.1	2.9
ER-20-6-1, 733	F	0.369	23.8	12.7	10.5	5.1
ER-20-6-1, 857	G	0.303	22.9	12.7	10.5	–
ER-20-6-1, 869	H	0.111	15.2	12.7	8.6	2.9

because of their importance to the interpretations and conclusions of this paper.

[13] All of the lab and field tracer experiments involved the “simultaneous” injection of a pair of nonsorbing tracers with different diffusion coefficients, a halide ion (either bromide or iodide) and pentafluorobenzoate (PFBA). The halides have free water diffusion coefficients of 2.0×10^{-5} to 2.1×10^{-5} cm²/s [Newman, 1973], and the PFBA has a free water diffusion coefficient of $\sim 7.6 \times 10^{-6}$ cm²/s [Bowman, 1984; Farnham *et al.*, 1997]; that is, a difference of a factor of ~ 3 . The differences in diffusion coefficients of these nonsorbing tracers provide the constraint necessary to distinguish the effects of matrix diffusion from the effects of advection, dispersion, and source tailing (artificial tailing because of delayed release of tracer from the injection region into the fracture flow system), all of which can result in apparent matrix diffusion behavior in a single tracer response [Callahan *et al.*, 2000; Becker and Shapiro, 2000]. Even in static diffusion cell experiments, inadvertent advective transport of the tracers (caused by injection and sampling procedures, or barometric cycling) can be recognized much more readily when multiple tracer breakthrough curves are obtained as opposed to a single tracer breakthrough curve. The underlying assumption in the multiple-tracer interpretative approach is that the simultaneously injected tracers all follow exactly the same flow pathways and are subjected to the same hydrologic conditions (including transients), so they experience identical transport parameters in the system except for the differences in $\frac{\phi_m}{b} \sqrt{D_m}$ caused by different matrix diffusion coefficients.

[14] To implement this interpretive approach, the laboratory fracture and field tracer transport experiments were analyzed using equations (1) and (2) with appropriate boundary conditions to “simultaneously” fit the normalized breakthrough curves (concentrations divided by injection masses or concentrations versus time) of the two nonsorbing tracers. The fits were obtained using the RELAP computer model [Reimus *et al.*, 2003b]. For each transport experiment, a single value of the mean water residence time (τ , hr) and the Peclet number (L / α , where L is transport distance and α is longitudinal dispersivity) was assumed to apply to both nonsorbing tracers, and the ratio of $\frac{\phi_m}{b} \sqrt{D_m}$ for the two tracers was always kept equal to $\sqrt{3}$ to maintain the ratio of the tracer free-water diffusion coefficients (assumed to be the ratio of the matrix diffusion coefficients, as justified by the data of Table 2). Assumptions regarding whether the matrix was a semi-infinite domain (infinite fracture spacing) or a finite domain (with specific fracture spacing) were also applied uniformly to both tracers. Breakthrough curves from

the longer residence time tests in the C wells cores were interpreted assuming a finite fracture spacing because the timescales of these tests were long enough that the tracers could have diffused to the no-flux boundaries at the periphery of the 8.9-cm-diameter cores (according to $\sqrt{2D_m\tau}$) and also because the breakthrough curves exhibited characteristics consistent with the tracers reaching a no-flux boundary in the matrix (as indicated by much better model fits assuming a finite matrix). Finally, for the field tests, the fractional tracer mass participation in each test was kept the same for both tracers. This parameter was allowed to vary to fit the field tracer breakthrough curves because of the many factors that can result in incomplete tracer recoveries in open systems [Reimus *et al.*, 2003a, 2003b]. Thus, all transport parameters for the two nonsorbing tracers with different diffusion coefficients were identical except for the $\sqrt{3}$ difference in the $\frac{\phi_m}{b} \sqrt{D_m}$ values.

[15] It should be noted that the apertures in the laboratory fractures were probably greater than they would have been under natural conditions because they were encapsulated in an epoxy flow apparatus with no confining pressure, and the shrinkage of the epoxy during curing likely resulted in the apertures opening slightly. The experiments were not designed to vary apertures or study aperture variance with applied stress. However, apertures and aperture distributions may have varied slightly in different experiments in the same fracture because of pressure fluctuations during and between tests that could have caused aperture field changes.

3. Results

[16] The properties and dimensions of the cores used in the laboratory fracture and diffusion cell experiments are listed in Tables 1 and 2, respectively. The flow rates associated with the tracer experiments conducted in each fracture are also listed in Table 1, and the diffusion coefficients determined in the diffusion cell experiments are listed in Table 2. Multiple diffusion cell experiments on different subsamples were conducted for several of the intervals to assess diffusion coefficient variability due to matrix variability. The matrix properties listed in Table 2 should effectively span the range of properties encountered in the field transport experiments at each location, as each sample came from within a field test interval.

[17] Figure 2 shows the RELAP model fits to the tracer breakthrough curves in the four C wells fractured cores on plots with log-log axis scales. Figure 3 shows similar plots for the four ER-20-6-1 fractured cores. The volumes of the tracer pulses were all approximately 50 mL, so the injection

Table 2. Properties and Dimensions of Core Samples Used in Diffusion Cell Experiments, and Halide and PFBA Matrix Diffusion Coefficients Measured in These Experiments

Diffusion Cell Sample Well, Depth, m bgs	Matrix Porosity	Matrix Permeability, m ²	Sample Thickness, cm	Sample Cross-Sectional Area, cm ²	Halide ^a Matrix Diffusion Coefficient, 10 ⁶ cm ² /s	PFBA Matrix Diffusion Coefficient, 10 ⁶ cm ² /s
UE-25C-2, 533	0.272	4.66E-15	0.98	79.4	6.2	2.0
UE-25C-2, 553	0.138	7.76E-19	1.23	79.7	0.38	0.13
UE-25C-1, 573 (1)	0.288	4.49E-16	2.27	79.4	3.0	1.1
UE-25C-1, 573 (2)	0.288	4.49E-16	1.82	20.08	2.8	1.0
UE-25C-1, 795	0.298	9.37E-17	0.79	75.9	1.0	0.35
ER-20-6-1, 682 (1)	0.297	3.95E-18	2.19	44.89	0.40	0.175
ER-20-6-1, 682 (2)	0.297	4.94E-18	2.14	44.89	0.45	0.2
ER-20-6-1, 682 (3)	0.297	1.97E-18	1.06	40.45	0.55	0.2
ER-20-6-1, 733 (1)	0.369	3.36E-17	1.50	20.27	2.55	0.85
ER-20-6-1, 733 (2)	0.369	3.06E-17	1.52	20.27	2.55	0.88
ER-20-6-1, 733 (3)	0.369	2.76E-17	2.33	137.9	3.15	1.15
ER-20-6-1, 733 (4)	0.369	3.06E-17	2.32	137.9	3.15	1.15
ER-20-6-1, 857 (1)	0.303	7.04E-15	2.34	42.89	4.3	1.6
ER-20-6-1, 857 (2)	0.303	3.25E-15	3.20	44.5	2.8	1.1
ER-20-6-1, 857 (3)	0.303	8.26E-15	2.70	19.91	3.9	1.45
ER-20-6-1, 869 (1)	0.111	2.37E-17	1.27	20.27	0.33	0.08
ER-20-6-1, 869 (2)	0.111	3.95E-18	1.14	19.75	0.09	0.018

^aBromide was used in C wells diffusion cells, and iodide was used in ER-20-6-1 diffusion cells.

pulse durations (in hours) in all experiments were approximately 50 divided by the flow rates listed in Table 1. The model fits in both figures could undoubtedly have been improved if a more sophisticated model had been employed in which fracture apertures, and hence values of $\frac{\phi_m}{b} \sqrt{D_m}$ were allowed to vary (for instance to account for spatially

varying apertures and hence spatially varying diffusion rates). The least squares fitting procedure was not artificially weighted, so it was inherently biased toward fitting the peak tracer concentrations, and more importantly, the “differences” in peak concentrations, better than the tail concentrations (note that the fits to the tails appear to be poorer

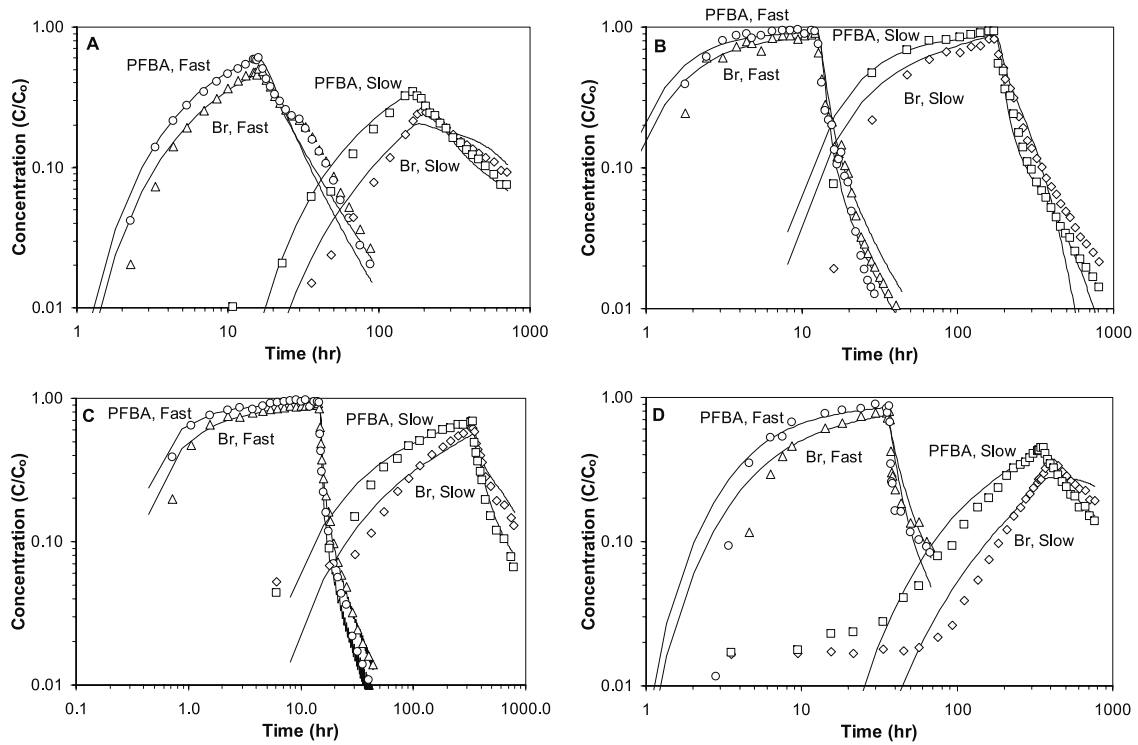


Figure 2. Normalized tracer breakthrough curves and best fit model curves for the eight paired tracer experiments conducted in the four naturally fractured cores from the C wells. Letters correspond to fracture designators listed in Tables 1 and 3. Best fitting transport parameters are listed in Table 3. “Fast” and “slow” refer to the higher and lower flow rates at which the transport experiments were conducted (Table 1). The early breakthroughs for the slow flow experiment in core D are attributed to residual tracer concentrations from the fast flow experiment in this core.

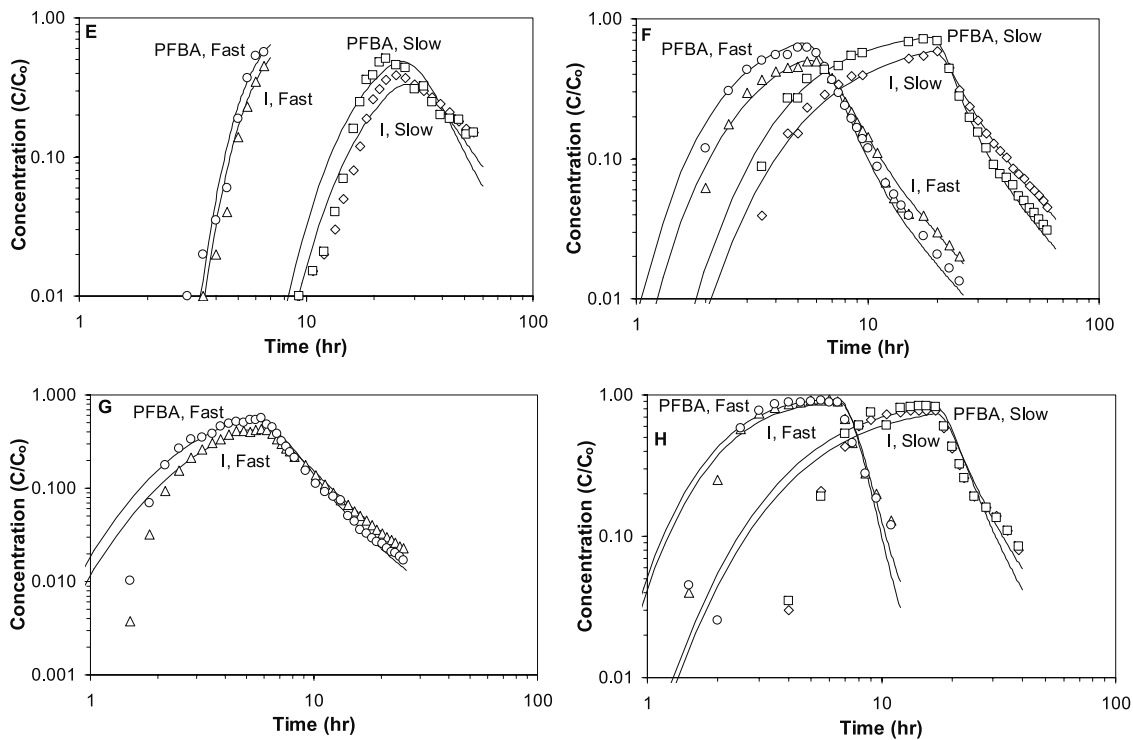


Figure 3. Normalized tracer breakthrough curves and best fit model results for the eight paired tracer experiments conducted in the four naturally fractured cores from ER-20-6-1. Letters correspond to fracture designators listed in Tables 1 and 3. Best fitting transport parameters are listed in Table 3. “Fast” and “slow” refer to the higher and lower flow rates at which the transport experiments were conducted (see Table 1).

than the fits to the peaks in Figures 2 and 3). Thus, the resulting estimates of $\frac{\phi_m}{b} \sqrt{D_m}$ are considered most representative of the fastest flow pathways through the fractures (the pathways that resulted in the peaks) and less representative of the slower flowing pathways.

[18] Table 3 lists the transport parameter estimates obtained from the laboratory fracture transport experiments, and Table 4 lists the parameter estimates obtained from the field transport experiments. The field test interpretations are taken from the works of *Reimus et al.* [2003a] and *Reimus and Haga* [1999].

[19] Figure 4 shows plots of $\frac{\phi_m}{b} \sqrt{D_m}$ for the halides (either bromide or iodide) as a function of both mean tracer residence time and transport length scale in the laboratory and field transport experiments. The laboratory data in both plots are presented as lines that connect the different mass transfer coefficients determined from experiments conducted in the same fracture at different flow rates (and hence different timescales). The lines associated with the field data in Figure 4a (the residence time plot) represent the uncertainty in tracer mean residence time that results from assuming either a radial (velocity a function of $1/r$, where r

Table 3. Transport Parameters Obtained From RELAP Fits to the Tracer Breakthrough Curves in the Laboratory Fracture Transport Experiments^a

Fractured Core Well, Depth, m bgs	Figures 2–5 Designator	Mean Residence Time, hr, Fast/Slow	Peclet Number Fast/Slow	Halide $\frac{\phi_m}{b} \sqrt{D_m}$ (sec ^{1/2}) Fast/Slow	Fracture Half-Aperture ^b from $b = Q\tau / 2LW$, cm Fast/Slow
UE-25C-2, 533 ^c	A	7.6/58	3.5/2.5	0.0086/0.0095	0.097/0.094
UE-25C-2, 553 ^c	B	1.4/19.6	7/7	0.0097/0.0041	0.025/0.026
UE-25C-1, 573 ^c	C	0.5/11	9/9	0.0230/0.0235	0.026/0.023
UE-25C-1, 795 ^c	D	4.0/46	5/6	0.010/0.014	0.049/0.052
ER-20-6-1, 682	E	4.6/16.2	50/14	0.003/0.0045	0.065/0.073
ER-20-6-1, 733	F	1.3/3.5	22/8	0.020/0.014	0.023/0.030
ER-20-6-1, 857	G	1.2	14	0.014	0.038
ER-20-6-1, 869	H	1.2/5.2	14/2.8	0.0048/0.0046	0.027/0.039

^aThe two values (xx/yy) listed for each parameter correspond to the fast and slow flow rate experiments, respectively.

^bDifferences in these half-aperture estimates are indicative of calculated mean residence times that are not strictly inversely proportional to volumetric flow rates.

^cA finite matrix with a no-flux boundary at 1.3 cm (A), 0.8 cm (B), 4.4 cm (C), and 2.0 cm (D) was assumed for the slower flow rate experiments in these four fractures. The matrix was assumed to be semi-infinite for all other experiments.

Table 4. Model Parameters Obtained From RELAP Fits to the Field Tracer Breakthrough Curves [Reimus et al., 2003a; Reimus and Haga, 1999]

Experiment	Tracer Mass Fraction	τ , hr ^a	Pe (-) ^b	Halide $\frac{\phi_m}{b} \sqrt{D_m}$ (sec ^{-1/2})
C wells Test 1, Pathway 1 ^c	0.115	30–36	6.5–9.3	0.0015
C wells Test 1, Pathway 2 ^c	0.60	630–1020	1.6–2.8	0.00047
C wells Test 2	0.72	610–1210	1.3–4.8	0.00095
ER-20-6 (1–3)	0.20	1600–1950	4.5–6.3	0.00049
ER-20-6 (1–2) ^d	0.005	210–300	2.8–4.5	0.00024

^aAssuming “radial” flow (smaller value) and “linear” flow (larger value) conditions.

^bAssuming linear flow (larger value) and radial flow (larger value) conditions.

^cTwo tracer peaks were observed, so test was interpreted assuming two transport pathways [Reimus et al., 2003a].

^dER-20-6-3 was the production well, with ER-20-6-2 being sampled at a very low rate [Reimus and Haga, 1999].

is distance from production well) or a linear (constant velocity) flow field. The mean residence time plot has more evenly spaced data points than the length scale plot because the residence times in the laboratory fracture experiments were varied through the use of different flow rates so that the longer laboratory residence times approached or overlapped the field residence times. The data in Figures 4a and 4b indicate that there is an apparent decreasing trend of $\frac{\phi_m}{b} \sqrt{D_m}$ with increasing tracer residence times and transport distances. However, it is also apparent that these trends are less obvious when the laboratory and field data are considered separately from each other.

[20] We examine matrix diffusion scaling behavior further by comparing the apparent matrix diffusion coefficients in the laboratory fracture and diffusion cell experiments conducted over different timescales using core material from the same interval. A systematic decrease in apparent matrix diffusion rates with time in these experiments could suggest a decreasing trend in matrix porosity or increasing matrix tortuosity from the surfaces to the interior of the matrix samples, which would translate into a decrease of diffusion rates with time. Although a direct comparison between the fracture and diffusion cell results is not strictly possible because the fracture experiments yield estimates of $\frac{\phi_m}{b} \sqrt{D_m}$, while the diffusion cell experiments yield estimates of D_m , we can calculate an equivalent matrix diffusion coefficient for the fracture experiments by assuming a parallel-plate fracture with a half aperture given by $Q\tau / 2LW$, where Q = volumetric flow rate through fracture (mL/hr), τ = mean residence time in fracture (hr), L = fracture length (cm), and W = fracture width (cm). This estimate of half aperture can then be squared, multiplied by the square of $\frac{\phi_m}{b} \sqrt{D_m}$, and divided by the square of the matrix porosity to obtain an estimate of D_m .

[21] The resulting D_m estimates are plotted with D_m estimates from the diffusion cell experiments (for bromide and iodide) as a function of residence time in Figure 5. The residence times associated with the diffusion cell experiments are assumed to be the time at which the tracer concentration on the low concentration side of the diffusion cell reached half of its final concentration (a value that was approximated in some cases). We note that this comparative approach yields the “minimum” possible matrix diffusion coefficients for the fracture experiments because any flow channeling in the fractures would have resulted in an effective fracture half aperture greater than what was calculated assuming parallel-

plate fractures. For instance, if flow channeling was such that only 25% of the surface area of the fractures was exposed to significant flow, then the effective half aperture in the fracture experiments would be four times larger and the calculated matrix diffusion coefficient for the fractures would be increased by a factor of 2.

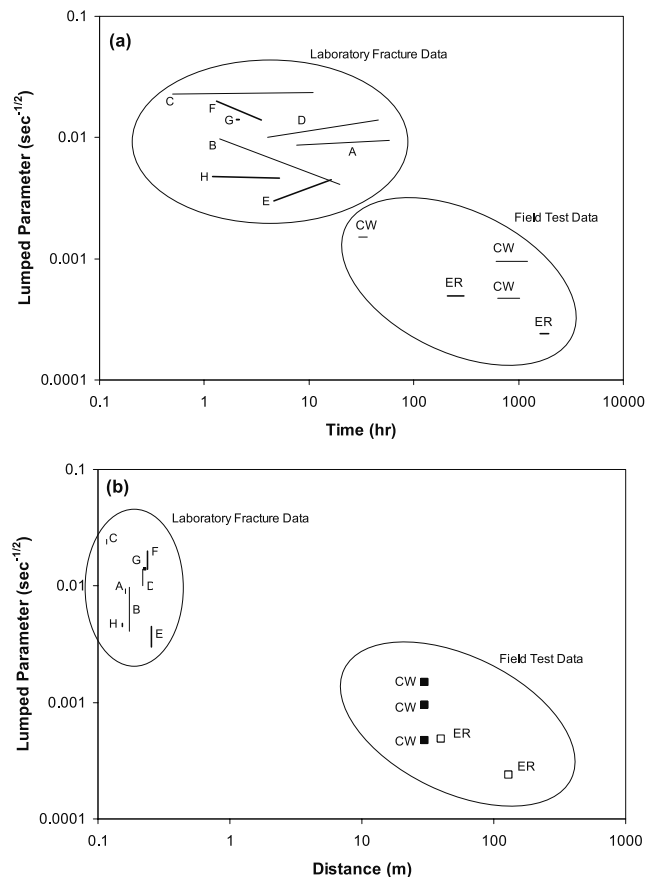


Figure 4. Lumped matrix diffusion mass transfer parameter $\frac{\phi_m}{b} \sqrt{D_m}$ as a function of (a) time and (b) distance scales in the laboratory and field tracer transport experiments. Letters correspond to laboratory fracture designators listed in Tables 1 and 3. Bold lines and dark squares correspond to data from the C wells site (CW), and lighter lines and open squares correspond to data from the ER-20-6 site (ER).

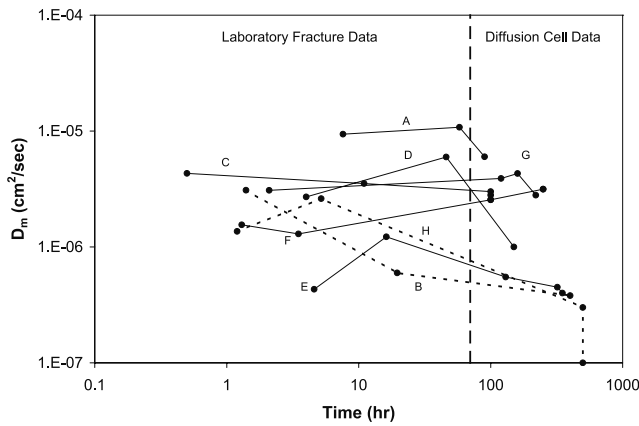


Figure 5. Matrix diffusion coefficients calculated from laboratory fracture experiments (assuming $b = Q\tau / 2LW$) and from diffusion cell experiments as a function of timescale. Letters correspond to laboratory fracture designators listed in Tables 1 and 3. Solid lines correspond to intervals with matrix porosities greater than 0.25, and dashed lines correspond to intervals with matrix porosities less than 0.15.

[22] Given these considerations, Figure 5 indicates that the matrix diffusion coefficients obtained from the fracture experiments are somewhat larger than those from the diffusion cells for the two lower matrix porosity rocks, but there is no consistent dependence of D_m for the higher matrix porosity rocks. Hypotheses explaining the apparent trend for the lower porosity rocks are (1) a portion of the solute diffusion in these fractures occurred within stagnant free water rather than in the true matrix, or (2) there was a significant gradient in porosity (decreasing) or tortuosity (increasing) from the matrix surfaces to the interior of these rocks, thus resulting in a decrease in matrix diffusion coefficients with distance into the rocks. Both processes would tend to be more pronounced and result in a greater time-scale dependence of D_m in lower porosity rocks than higher-porosity rocks. We had previously suspected that some of the apparent scale dependence of matrix diffusion rates in Figure 4 might be attributable to such processes, but Figure 5 indicates that while these processes may be real, they are not significant enough to fully explain the trends of Figure 4 (note that D_m must decrease by 2 orders of magnitude to explain a 1 order-of-magnitude decrease in $\frac{\phi_m}{b} \sqrt{D_m}$).

4. Discussion and Conclusions

[23] Figure 4 indicates that matrix diffusion mass transfer rates in fractured volcanic media at the NTS appear to decrease with both time and distance scales. However, the lack of a clear trend of matrix diffusion coefficients with time for the higher matrix porosity rocks in the laboratory experiments (Figure 5), coupled with the fact that the laboratory values of $\frac{\phi_m}{b} \sqrt{D_m}$ are consistently larger than the field values even when the timescales in the laboratory fracture experiments are increased to the point where they overlap with the field experiment timescales, argues for a greater influence of distance scales in explaining the significantly different values of $\frac{\phi_m}{b} \sqrt{D_m}$ obtained from the lab- and field-scale experiments.

[24] The only logical explanation for the approximately 1 order-of-magnitude smaller values of $\frac{\phi_m}{b} \sqrt{D_m}$ in the field-scale tests compared to the laboratory-scale tests (Figure 4) is that the effective fracture apertures in the field tests were significantly larger than in the laboratory tests. Given that the range of matrix porosities in all the laboratory samples (and also from borehole geophysical logging measurements [e.g., Gelson, 1993]) ranged from ~ 0.10 to ~ 0.35 , it seems very unlikely that the smaller value of $\frac{\phi_m}{b} \sqrt{D_m}$ at the field scale could be a result of matrix porosities as low as $0.01 - 0.035$. It also seems unlikely that matrix diffusion coefficients could be a factor of 100 lower in the field experiments than in the lab experiments. Even the simultaneous lowering of these two parameters to the point where the field estimates of $\frac{\phi_m}{b} \sqrt{D_m}$ are matched would put their values well outside the range of existing data. Indeed, the rocks of lowest matrix porosity in the laboratory experiments, which also had the lowest matrix diffusion coefficients, had $\frac{\phi_m}{b} \sqrt{D_m}$ values that were still much larger than the field values (Figure 4). These rocks were selected to be representative of the lithologies with the lowest possible matrix diffusion rates in the field test intervals based on their matrix porosities and expected values of matrix diffusion coefficients.

[25] In contrast, an order-of-magnitude increase in effective fracture apertures at the field scale relative to the laboratory scale seems very plausible. Flow will naturally tend to focus in larger-aperture fractures or larger-aperture channels within fractures, which offer less flow resistance than lower aperture regions. As length scales increase, contaminants will tend to have a greater probability of encountering these larger-aperture flow features and a greater tendency to remain in these features (or to move from one to another if they are not fully connected). It is extremely unlikely that the small-scale laboratory fractures, particularly the induced ones, were representative of the dominant features that transmit flow between the field boreholes over distances of 30 m or more. Indeed, despite the fact that the laboratory fractures probably had greater apertures than if an active confining pressure were applied (because of the epoxy shrinkage), the apertures in the cores were still apparently much smaller than effective apertures that tracers experienced in the field tests.

[26] This line of reasoning is supported by several indirect lines of evidence. First, borehole flow surveys at the NTS [Bechtel-SAIC Corporation, 2004b] typically indicate that only a small fraction of the visible fractures in any borehole transmit water to any significant degree. Thus, the probability of intersecting a major flowing feature in a borehole core sample is exceedingly small, and even the probability of an entire borehole intersecting such a flow feature may be quite small if the features are steeply dipping, as fractures at the NTS tend to be at many locations, including the C wells [Gelson, 1993]. If flow occurs primarily in approximately one-dimensional channels within fracture networks rather than in two-dimensional planar features, as some have speculated [e.g., Neuzil and Tracy, 1981; Moreno et al., 1990; Thompson, 1991; Moreno and Tsang, 1994; Gentier et al., 2000], the probability of a borehole intersecting a flow feature will be even less. Second, a small number fractures intersecting NTS boreholes appear to have apertures of several centimeters

(evident from borehole televiewer and television logs), which is consistent with field-estimated values of $\frac{\phi_m}{b} \sqrt{D_m}$ coupled with lab-estimated values of ϕ and D_m . These large-aperture fractures often do not transmit much flow into or through boreholes, but they clearly exist, and they presumably could transmit a considerable amount of flow if properly connected to the flow system. Third, single-well hydraulic tests in fractured rocks at the NTS tend to yield lower transmissivity estimates, even after accounting for well losses, than corresponding cross-hole hydraulic tests. At the C wells, single-well pumping tests yielded transmissivity estimates between 1 and 2 orders of magnitude lower than cross-hole tests [Geldon, 1996], and at the ER-20-6 complex, the single-well test transmissivities were a factor of 3–8 lower than cross-hole tests [IT, 1997]. These results suggest that while the most conductive flow features at the NTS are sparse enough that they are generally not intersected by individual boreholes, they occur with enough frequency that their effects are usually reflected in cross-hole hydraulic responses [Geldon, 1996]. All of these observations are consistent with smaller values of $\frac{\phi_m}{b} \sqrt{D_m}$ being observed at field scales compared to lab scales.

[27] Other potential explanations for smaller observed values of $\frac{\phi_m}{b} \sqrt{D_m}$ at field scales than lab scales cannot be ruled out. Such explanations include (1) the possible presence of fracture coating minerals that could act as diffusion barriers in the field but are not present in core samples and (2) the possibility of a small amount of advective flow from the matrix into fractures in the field caused by the significant lowering of fracture pressures near the production well, which would counteract matrix diffusion (although lowering of pressure would also tend to decrease apertures, which should enhance diffusive mass transfer rates). However, there is no direct evidence that fracture coatings result in tight diffusion barriers (available data suggest they have little effect on diffusion [Reimus *et al.*, 2002b]), and any advective flow from matrix to fractures should have been minimized by allowing pressures and flow rates to stabilize before tracers were injected in field tests. In fact, the tracer injection process might be expected to result in a small amount of advective flow into the matrix (enhancing matrix diffusion) near the injection borehole because of the elevated pressures associated with injection (although the increased pressures would also increase apertures, thus slowing down diffusion rates).

[28] Thus, careful consideration of the laboratory and field data points toward a dominant role of effective fracture apertures in dictating how matrix diffusion rates (as reflected by values of $\frac{\phi_m}{b} \sqrt{D_m}$) will scale with time and distance in fractured volcanic rocks at the NTS. Moreno and Neretnieks [1993] reached a similar conclusion in crystalline rocks. There is no logical reason to expect a scale dependence of matrix porosities for a given lithology, and the laboratory diffusion cell and fracture transport experiments show no conclusive evidence of a timescale dependence of matrix diffusion coefficients in higher matrix porosity rocks. Also, matrix porosities and matrix diffusion coefficients would have to assume values much smaller than the lower limits of their independently measured ranges to account for the significantly smaller values of $\frac{\phi_m}{b} \sqrt{D_m}$ in field-scale tests relative to laboratory-scale tests.

[29] We conclude that while the available data from the NTS suggest a trend of decreasing matrix diffusion rates with time and distance scales, these trends are likely dominated by variations in effective fracture apertures in the different tests. Field tracer tests of larger distance scales tend to have much larger apertures and thus smaller values of $\frac{\phi_m}{b} \sqrt{D_m}$ than laboratory tracer tests. Any apparent trend with timescale is probably a consequence of the positive correlation between distance and timescales, although the laboratory tests at different timescales suggest that there could be a decrease in $\frac{\phi_m}{b} \sqrt{D_m}$ with increasing timescale for rocks of matrix porosity less than 0.15, possibly because of a larger gradient of matrix porosity and tortuosity between the surface and interior of these rocks compared to higher-porosity rocks.

[30] These results underscore the importance of acquiring a better understanding of the factors that control effective fracture apertures as a function of distance scale if matrix diffusion rates are to be reliably extrapolated from laboratory and field tracer tests to risk assessment time and distance scales in fractured media. It is conceivable that effective fracture apertures could increase or decrease with distance depending on several site-specific factors, including (1) whether the source starts out in a portion of the flow system that has large or small apertures relative to the rest of the system, (2) whether flow tends to diverge from or converge toward large flow features, and (3) what the characteristic length scales of large flow features are relative to the length scale of the overall flow system. These factors undoubtedly have many underlying dependencies such as the geologic evolution and stress-strain history of the rock, the overall structural and hydrogeologic setting, the mechanical properties of the rock matrix, and any rock-water interactions.

[31] Finally, it is important to recognize that, beyond some critical time and distance scale in a given flow system, matrix diffusion scaling behavior will transition from being mainly dependent on matrix diffusion “rates” to being mainly dependent on diffusion “length scales” (for example, flowing fracture spacings, matrix block sizes). Thus, for long time and distance scales, effective fracture apertures and their scale dependence may ultimately not be as critical in contaminant transport risk assessments as determining (1) the time of transition from diffusion-rate-dominated scaling behavior to diffusion-length-dominated scaling behavior and (2) the values of the diffusion-length-scale parameters in the system of interest.

[32] **Acknowledgments.** We thank Robert Bowman, John Wilson, Brian McPherson, and Fred Phillips for their thoughtful discussions of this work and suggestions on interpreting the data, Marc Haga for conducting the diffusion cell experiments, Andy Humphrey for conducting the ER-20-6-1 fracture transport experiments, and Dale Counce for conducting the sample analyses. We also thank the associate editor and three anonymous reviewers for their thoughtful reviews, which significantly improved this manuscript. This work was supported in part by the US Department of Energy Office of Civilian Radioactive Waste Management. The work was also supported in part by the US Department of Energy Underground Test Area Program, managed out of the National Nuclear Security Administration’s Nevada Area Office.

References

Bajracharya, K., and D. A. Barry (1997), Nonequilibrium solute transport parameters and their physical significance: Numerical and experimental results, *J. Contam. Hydrol.*, 24, 185–204.

- Bechtel-SAIC Corporation (2004a), *Saturated Zone In-Situ Testing*, ANL-NBS-HS-000039, Rev. 01, Yucca Mountain Project Analysis Report, Bechtel-SAIC, Las Vegas, Nevada. (available for viewing at <http://www.lsnnet.gov/>)
- Bechtel-SAIC Corporation (2004b), *Probability Distribution for Flowing Interval Spacing*, ANL-NBS-MD-000003, Rev. 01, Yucca Mountain Project Analysis Report, Bechtel-SAIC, Las Vegas, Nevada. (available for viewing at <http://www.lsnnet.gov/>)
- Becker, M. W., and A. M. Shapiro (2000), Tracer transport in fractured crystalline rock: Evidence of nondiffusive breakthrough tailing, *Water Resour. Res.*, 36(7), 1677–1686.
- Bowman, R. S. (1984), Evaluation of some new tracers for soil water studies, *Soil Sci. Soc. Am. J.*, 48(5), 987–993.
- Callahan, T. J. (2001), Laboratory investigations and analytical and numerical modeling of the transport of dissolved solutes through fractured rock, Ph.D. dissertation, New Mexico Institute of Mining and Technology, Socorro, New Mexico.
- Callahan, T. J., P. W. Reimus, R. S. Bowman, and M. J. Haga (2000), Using multiple experimental methods to determine fracture/matrix interactions and dispersion in saturated fractured volcanic tuff, *Water Resour. Res.*, 36(12), 3547–3558.
- Farnham, I. M., L. C. Meigs, M. E. Dominguez, K. Lindley, J. M. Daniels, and K. J. Stetzenbach (1997), Evaluation of tracers used for the WIPP tracer tests, Appendix H in *Interpretations of Tracer Tests Performed in the Calebra Dolomite at the Waste Isolation Pilot Plant Site*, edited by L. C. Meigs, R. L. Beauheim, and T. L. Jones, SAND97-3109, Sandia National Laboratories, Albuquerque, NM.
- Geldon, A. L. (1993), Preliminary Hydrogeologic Assessment of Boreholes UE-25c #1, UE-25c #2, and UE-25c #3, Yucca Mountain, Nye County, Nevada, *Water-Resources Investigations Report 92-4016*, US Geological Survey, Denver, Colorado.
- Geldon, A. L. (1996), Results and Interpretations of Preliminary Aquifer Tests in Boreholes UE-25c #1, UE-25c #2, and UE-25c #3, Yucca Mountain, Nye County, Nevada, *Water-Resources Investigations Report 94-4177*, US Geological Survey, Denver, Colorado.
- Gentier, S., D. Hopkins, J. Riss (2000), Role of fracture geometry in the evolution of flow paths under stress, in *Dynamics of Fluids in Fractured Rock*, *Geophys. Monogr.* 122, AGU, Washington, D. C.
- Grisak, G. E., and J. F. Picketts (1980), Solute transport through fractured media: 1. The effect of matrix diffusion., *Water Resour. Res.*, 16, 719–730.
- Haggerty, R., and S. Gorelick (1995), Multiple-rate mass transfer for modeling diffusion and surface reactions in media with pore-scale heterogeneity, *Water Resour. Res.*, 31(10), 2383–2400.
- International Technology (IT) Corporation (1997), BULLION Forced-Gradient Experiment Implementation Plan. *ITLV/10972-195*. Las Vegas, Nevada.
- International Technology (IT) Corporation (1998), Report and Analysis of the BULLION Forced Gradient Experiment. *DOE/NV/13052-042*. Las Vegas, Nevada.
- Lichtner, P. C. (2000), Critique of dual continuum formulations of multi-component reactive transport in fractured porous media, in *Dynamics of Fluids in Fractured Rock*, edited by B. Faybishenko, P. A. Witherspoon, and S. M. Benson, *Geophys. Mon.*, 122, 281-298, AGU, Washington, D. C.
- Maloszewski, P., and A. Zuber (1984), Interpretation of artificial and environmental tracers in fissured rocks with a porous matrix. In *Isotope Hydrology*, pp. 635-651, International Atomic Energy Agency, IAEA, Vienna, Austria.
- Maraq, M. A., R. B. Wallace, and T. C. Voice (1999), Effects of residence time and degree of water saturation on sorption nonequilibrium parameters, *J. Contam. Hydrol.*, 36, 53–72.
- Moreno, L., C-F. Tsang, Y. Tsang, and I. Neretnieks (1990), Some anomalous features of flow and solute transport arising from fracture aperture variability, *Water Resour. Res.*, 26(10), 2377–2391.
- Moreno, L., and I. Neretnieks (1993), Flow and nuclide transport in fractured media: The importance of the flow-wetted surface for radionuclide migration, *J. Contam. Hydrol.*, 13, 49–71.
- Moreno, L., and C-F. Tsang (1994), Flow channeling in strongly heterogeneous porous-media—A numerical study., *Water Resour. Res.*, 30(5), 1421–1430.
- Neretnieks, I. (1980), Diffusion in the rock matrix: An important factor in radionuclide retardation, *J. Geophys. Res.*, 85, 4379–4397.
- Neuzil, C. E., and J. V. Tracy (1981), Flow through fractures, *Water Resour. Res.*, 17, 191–199.
- Newman, J. (1973), *Electrochemical Systems*, Prentice-Hall, Upper Saddle River, N. J.
- Rao, P. S. C., R. E. Jessup, D. E. Rolston, J. M. Davidson, and D. P. Kilcrease (1980), Experimental and mathematical description of nonadsorbed solute transfer by diffusion in spherical aggregates, *Soil Sci. Soc. Am. J.*, 44, 684–688.
- Reimus, P. W., and M. J. Haga (1999), Analysis of tracer responses in the BULLION forced-gradient experiment at Pahute Mesa, Nevada, Los Alamos National Laboratory Report LA-13615-MS, Los Alamos, NM.
- Reimus, P. W., S. D. Ware, F. C. Benedict, R. G. Warren, A. R. Humphrey, A. I. Adams, B. Wilson, and D. Gonzales (2002a), Diffusive and advective transport of ³H, ¹⁴C, and ⁹⁹Tc in saturated, fractured volcanic rocks from Pahute Mesa, Nevada. *LA-13891-MS*, Los Alamos National Laboratory, Los Alamos, NM.
- Reimus, P. W., M. J. Haga, A. R. Humphrey, D. A. Counce, T. J. Callahan, and S. D. Ware (2002b), Diffusion cell and fracture transport experiments to support interpretations of the BULLION forced-gradient experiment., *LA-UR-02-6884*, Los Alamos National Laboratory, Los Alamos, NM.
- Reimus, P. W., M. J. Haga, A. I. Adams, T. J. Callahan, H. J. Turin, and D. A. Counce (2003a), Testing and parameterizing a conceptual solute transport model in saturated fractured tuff using sorbing and nonsorbing tracers in cross-hole tracer tests, *J. Contam. Hydrol.*, 62-63, 613–626.
- Reimus, P. W., G. Pohll, T. Mihevc, J. Chapman, M. Haga, B. Lyles, S. Kosinski, R. Niswonger, and P. Sanders (2003b), Testing and parameterizing a conceptual model for solute transport in fractured granite using multiple tracers in a forced-gradient test, *Water Resour. Res.*, 39(12), 1356, doi:10.1029/2002WR001597.
- Robinson, B. A. (1994), A strategy for validating a conceptual model for radionuclide migration in the saturated zone beneath Yucca Mountain, *Radioact. Waste Manage. Environ. Restor.*, 19, 73–96.
- Tang, D. H., E. O. Frind, and E. A. Sudicky (1981), Contaminant transport in fractured porous media: Analytical solution for a single fracture, *Water Resour. Res.*, 17, 555–564.
- Thompson, M. E. (1991), Numerical simulation of solute transport in rough fractures, *J. Geophys. Res.*, 96(B3), 4157–4166.
- Toride, N., F. J. Leij, and M. Th. van Genuchten (1995), The CXTFIT code for estimating transport parameters from laboratory or field, Version 2.0, *U.S. Agric. Res. Rep.*, 138, 121pp.
- Tsang, Y. W. (1995), Study of alternative tracer tests in characterizing transport in fractured rocks, *Geophys. Res. Letters*, 22(11), 1421–1424.

T. J. Callahan, Department of Geology and Environmental Geosciences, College of Charleston, 66 George Street, Charleston, SC 29424, USA. (callahant@cofc.edu)

P. W. Reimus, Earth and Environmental Sciences Division, Los Alamos National Laboratory, MS J534, P.O. Box 1663, Los Alamos, NM 87545, USA. (preimus@lanl.gov)